Turk. J. Math. Comput. Sci.
15(2)(2023) 365–374

DOI : 10.47000/tjmcs.1249300

Skin Lesion Classification Using Convolutional Neural Network and ABCD Rule

Ezgi Kestek[1,*], Mehmet Emin Aktan[2,3], Erhan Akdoğan[1,2]

[1]*Department of Mechatronics Engineering, Faculty of Machinery, Yıldız Technical University, 34349, Istanbul, Türkiye.*
[2]*Health Institutes of Türkiye, 34718, Istanbul, Türkiye.*
[3]*Department of Mechatronics Eng., Faculty of Engineering, Architecture and Design, Bartın University, 74100, Bartın, Türkiye.*

Received: 09-02-2023 • Accepted: 06-11-2023

Abstract. Skin cancer, which can occur in any part of the human skin, is one of the common and serious types of cancer. Accurate diagnosis and segmentation of lesions are crucial to the early diagnosis. Computer-aided diagnosis make important contributions to help doctors in the diagnosis of cancer from skin images. The most important factor for such systems to reveal the accurate results is the correct feature extraction. In this study, a model for the classification of seven types of skin lesions is developed by combining the features of CNN-based feature extraction and the ABCD rule, which is widely used in the clinic. The model is evaluated on HAM10000 well-known dataset. The classification results obtained with different combinations of features and machine learning algorithms are compared. According to the results, the best classification accuracy is obtained with the Cosine Similarity Classifier with 96.4% when the features determined by CNN and the features in the ABCD rule are used together.

2020 AMS Classification: 65D19, 97R40

Keywords: Skin cancer, deep learning, convolutional neural network, classification, ABCD rule.

1. Introduction

Skin cancer is one of the most common and serious types of cancer affecting humans. One of the most important causes of skin cancer is harmful ultraviolet rays that occur with the depletion of the ozone layer [1]. There are two main types of skin cancer: melanoma and non-melanoma. The non-melanoma is much more common and less dangerous than melanoma [2–4]. The most prevalent types of non-melanoma are basal cell carcinoma (BCC) and squamous cell carcinoma (SCC). BCC, which is usually seen in the head and neck region, is the most common type of skin cancer (75-80%) [5]. Although melanoma is not very common compared to other types of skin cancer, its lethality is higher [6, 7]. In studies on future projections, it is anticipated that there will be a 50% increase in melanoma cases and a 68% increase in casualties in 2040 compared to 2020 [8].

The early diagnosis of melanoma is crutial for successful and effective treatment. While the survival rate is over 95% in early-diagnosed melanoma cases, the five-year survival rate drops below 15% in late diagnosis [9]. Most patients diagnosed with early-stage melanoma have localized lesions and are successfully treated with surgery [10]. In cases of melanoma that are detected in the late stage, spread beyond the skin occurs, and treatment becomes difficult. In this

*Corresponding Author
Email addresses: ezgi.kestek@gmail.com (E. Kestek), maktan@bartin.edu.tr (M.E. Aktan), eakdogan@yildiz.edu.tr (E. Akdoğan)

case, treatment methods such as surgical removal of melanoma-spreading tissues, immunotherapy, targeted therapy, chemotherapy, and radiation therapy are used [11, 12]. As in all other types of cancer, the crucial factor affecting the success of treatment in skin cancer and its dangerous type, melanoma, is early diagnosis [13, 14].

There is ample evidence that artificial intelligence (AI) and machine learning (ML) can help clinicians make better clinical decisions. Studies in the literature have shown that AI can outperform or equal to expert dermatologists [15–17]. Thanks to the ability of AI algorithms to process a large number of data rapidly and with high accuracy, it is possible to detect anomalies in various tissue images and thus to diagnose cancer cases at an early stage. In this context, there are many studies in the literature. Early research in this area attempted to apply low-level features such as color, shape and border to distinguish melanomatic lesions [18, 19]. This approach is older and conventional, using hand-crafted features designed by researchers to capture important visual features of the image. Some researchers have suggested using feature selection algorithms to identify suitable hand-crafted features that can be used in classification [20, 21]. However, these hand-crafted features fail to cope with the large number of variations of melanoma and the high degree of visual similarity between melanoma and non-melanoma lesions. In addition, it is seen that the artifacts in the images cause negative effects. Recently, convolutional neural networks (CNN) with feature extraction capability have made important contributions to medical image analysis, including diagnosis and classification [22–26]. Codella et al. [27] presented an approach for melanomatic lesion detection in 2624 dermoscopy images that combines CNN, sparse coding, and SVM learning algorithms. In this work, two discrimination tasks are examined: melanoma vs. all non-melanoma lesions, and melanoma vs. atypical lesions. The presented approach achieves an accuracy of 93.1% and 73.9% for the first and second tasks, respectively. Yu et al. [28] constructed a fully convolutional residual network (FCRN) for skin lesion segmentation and combined with very deep residual networks for classification. This method achieved an accuracy of 85.5%. Majtner et al. [29] proposed a melanoma detection method based on the CNN technique. In the study, in which CNN was used for feature extraction and preprocessing, the samples were divided into two classes as benign and malignant. LDA techniques were used for feature reduction and tested with 4 different classifiers. KNN provided the best accuracy with 86%. Acosta et al. [30] proposed a mask-based and region-based CNN model combined with a pretrained ResNet152 structure. The Mask RCNN was used to create a boundary box on the lesion and ResNet152 was used to lesion classification. The proposed method provided an accuracy of 90.4%. Afza et al. [31] proposed a model based on two-dimensional superpixels combined with deep learning. ResNet-50 was applied for the mapped images, and transfer learning was used for the learned features. The extracted features are optimized and classification performed. The proposed framework has been tested on three datasets (Ph2, ISBI2016, and HAM1000) and obtained an accuracy of 95.40%, 91.1%, and 85.50%, respectively. Jin et al. [32] developed a cascade knowledge diffusion network (CKDNet) for skin lesion segmentation. In the study using ISIC2017 and ISIC2018 datasets, 94.6% and 96.3% accuracy were obtained, respectively.

In this study, a model for the classification of seven types of skin lesions was developed by combining the features of CNN-based feature extraction and the ABCD rule, which is widely used in the clinic. The well-known and widely used HAM10000 dataset was used in the study. The classification results obtained with different combinations of features and nine different machine learning algorithms were compared. According to the results obtained, the best classification accuracy with 96.4% was obtained with the Cosine Similarity Classifier when the features obtained with CNN and the features in the ABCD rule were used together.

The proposed document is organized as follows: the first section introduces the problem, literature review and research aim, it is followed by the material and method, which describes dataset and preprocessing steps, and feature extraction methods. At the third section the results are presented, this is followed by a discussion. Finally, it is concluded with a general evaluation and future work suggestions.

2. Material and Method

2.1. **Dataset.** In this study, we used the open-source Skin Cancer MNIST: HAM10000 dataset [33]. The dataset consists of 10015 dermoscopic images of 7 types of pigmented skin lesions: actinic keratoses and intraepithelial carcinoma (327 images), basal cell carcinoma (514 images), benign keratosis-like lesions (1099 images), dermatofibroma (115 images), melanoma (1113 images), melanocytic nevi (6705 images), and vascular lesions (angiomas, angiokeratomas, pyogenic granulomas, and hemorrhage (142 images)). The patients were mostly between the ages of 35 and 70. The images are in 600x450 resolution and jpeg format. More than half of the lesions were confirmed by histopathology,

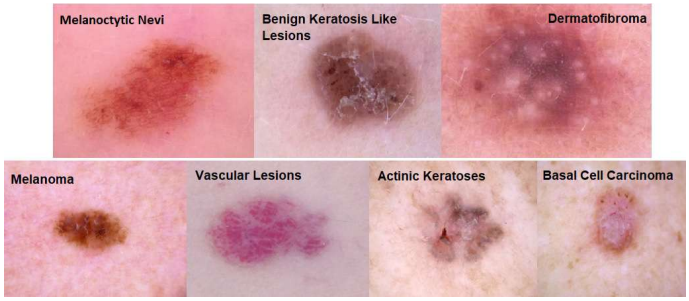

FIGURE 1. Sample images for the seven skin lesion types from the dataset.

with the remainder confirmed by follow-up examination, expert consensus or in vivo confocal microscopy. Fig. 1 shows a sample images from the HAM10000 dataset for each class.

2.2. **Preprocessing.** To improve the quality of the images and standardization, a 2-stage preprocessing process was applied. The first of these is the filtering process applied to remove objects such as noise, thick or thin hair, low contrast lesion, dark spot and air bubbles in the images. These artifacts prevent the boundaries from being obtained clearly during the thresholding process. In the literature, Gaussian, mean and median filters are frequently used in the preprocessing [34, 35]. In this work, after applying the mean filter, the bottom-hat filter with disk-shaped structural elements were applied. Secondly, segmentation was performed to determine the lesion area (Fig. 2). Thresholding is applied to the bottom-hat-filtered image with the Otsu method. Since the symmetry index will be required in the search process, the positions of the black and white pixels in the image have been changed by the imcomplement command. In addition, the stains around the lesion were removed by applying the closing operation. Finally, the segmentation was completed with the thickening operation. The Image Batch Processor in the MATLAB Image Processing Toolbox was used to apply the aforementioned preprocessing steps to the entire data set.

2.3. **Feature Extraction.** Different features from images were used to classify skin lesions. The effects of these features on classification accuracy were compared. In the study, asymmetry, border, color and diameter features in the ABCD rule together with 128 features obtained with CNN are the features used in the classification.

2.3.1. *Convolutional Neural Network.* CNN, which are a special type of Multi Layer Perceptron and created by modeling the human visual system, are widely used in the field of computer vision today. It is widely used in feature extraction from input data. CNN have been used to improve the performance in many image processing applications with various architectures such as ResNet, DenseNet, Xception, AlexNet, VGGNet, etc. In this study, Xception [36] CNN architecture, which has become popular in recent years and gives better results than other architectures in feature extraction from medical images, is used [37–39]. The Xception model is a 71-layer deep CNN, inspired by the Inception model from Google, that involves Depthwise Separable Convolution and residual structure. The 400x600 images in the dataset have been resized to 224 x 224 pixels on all layers to be compatible with the Xception architecture and then split into 7,010 images for training and 3,005 for testing. 128 features were determined with the CNN feature extraction model created with the Xception architecture.

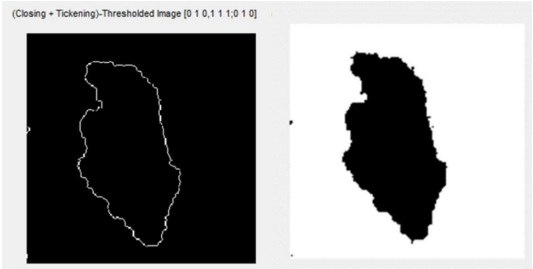

FIGURE 2. Image with segmentation applied.

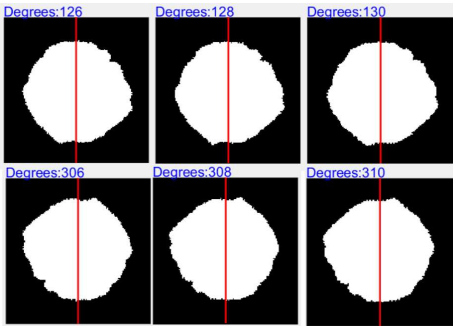

FIGURE 3. Symmetry lines at different angles in a malignant lesion image.

2.3.2. *ABCD Rule.* The ABCD rule is an acronym for the characteristics that doctors look for when diagnosing and classifying melanomatic lesions. These characteristics are asymmetry, border, color and diameter.

Asymmetry: The shape of the lesions in melanoma cases is not uniform but asymmetrical. Non-cancerous moles typically have a symmetrical appearance. To determine the asymmetry of the blob in the images, a thresholded and color-inverted image was used. The degree of symmetry of the lesions was calculated by the method suggested by T. Coye [40], using the Jaccard index. The image is rotated clockwise from 0 to 360 degrees in 2-degree steps, and A and A' obtained. Following, the Jaccard index and distance for A and A' are calculated. A symmetry line is drawn or not drawn depending on the distance. This is done at each rotation step. As a result of the process, the number of similarity lines of the image with the Jaccard index and Jaccard distances is obtained. The number of symmetry lines was found to be 3 for the image in the Fig. 3.

Border Irregularity: Melanomatic moles often have uncertain or irregular borders, while non-cancerous lesions usually have smooth borders. The most important parameters for examining the border irregularity in the preprocessed image are the total length (P) and the mean diameter (d) of the blob borders. In order to determine the border irregularity of the lesion, the image is divided into eight equal segments. In the ABCD rule, the border irregularity score between 0-8 is determined by evaluating the irregularity present in each of the eight segments. If there is no irregularity in any of the segments, 0 points are given. If there is irregularity in each segment, the border irregularity score is 8. Border irregularity score between 0 and 8 was calculated from the Katz Fractal dimension [41, 42]. The fractal dimension (D) of a planar curve is found by Eq. (2.1).

$$D = \frac{log(P)}{log(d)}, \tag{2.1}$$

where P is the total length of the curve and d is the diameter of the curve [41]. The Katz fractal dimension for the number of n digits across the lesion was determined by Eq. (2.2).

$$K_D = \frac{loglog(n)}{loglog(\frac{d}{P}) + loglog(n)}, \qquad n = \frac{P}{a}, \tag{2.2}$$

where a is the average step, i.e. the average distance between consecutive points in the time series, and n is the number are the steps in the time series [43].

For circular lesions, the irregularity of the lesion was determined from the deviation of the fractal size of that structure from the reference value, taking the fractal dimension of the circle as a reference.

Color: Melanoma lesions are often more than one color. Non-cancerous moles typically one color. Possible colors to be found in the lesion area are white, red, black, light brown, dark brown and blue-gray. The total color score values of the lesions were calculated by the method developed by T. Coye [44]. Points are given to each color in the lesion area. A total color score (TCS) is obtained by summing all color values (Eq. (2.3)). An example color score calculation interface is given in Fig. 4.

$$TCS = white + red + black + lightbrown + darkbrown + blue, gray > 0. \tag{2.3}$$

Diameter: Melanoma growths are normally larger than 6mm in diameter. Here, the diameter (d) value in the border irregularity calculation is used (Eq. (2.1)).

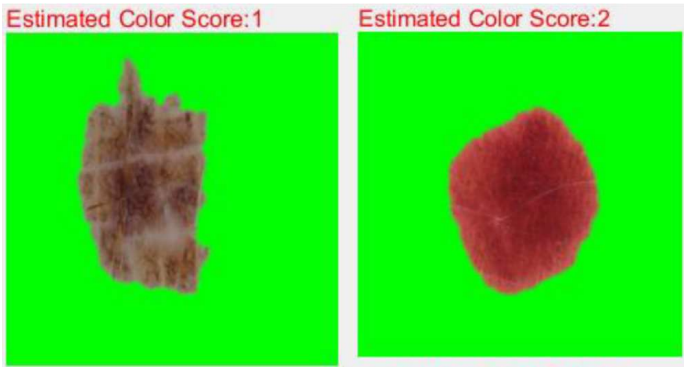

FIGURE 4. Color score calculation for two different malignant images.

The overview of the classification model including the CNN feature extraction structure and the ABCD rule is given in Fig. 5.

In the proposed architecture, the dataset first undergoes the data preprocessing steps outlined in the previous sections. During this process, all image data cleaned and converted into floating-point arrays. Subsequently, a CNN model is defined, and this model is constructed utilizing the Xception architecture. To be applied to the resulting data frame, the features are concatenated with the defined variable obtained from the last four layers of the model. The Xception model architecture is a pre-defined structure provided by Keras, which includes convolutional layers and max pooling layers. Max pooling reduces the size of feature maps. The obtained features undergo normalization using MATLAB functions. The data is partitioned into testing, training, and validation sets. Element-level addition is performed by adding each element in one feature tensor to the corresponding element in another feature tensor. This operation is employed to facilitate specific mathematical operations through the combination of feature tensors.

2.4. **Evaluation Metrics.** The calculation of true-positive (TP), true-negative (TN), false-positive (FP) and false-negative (FN) values is widely used in classification studies to measure the success of the model. True-positive and true-negative represent the correctly classified outputs for the target disease, respectively. Therefore, false-positive

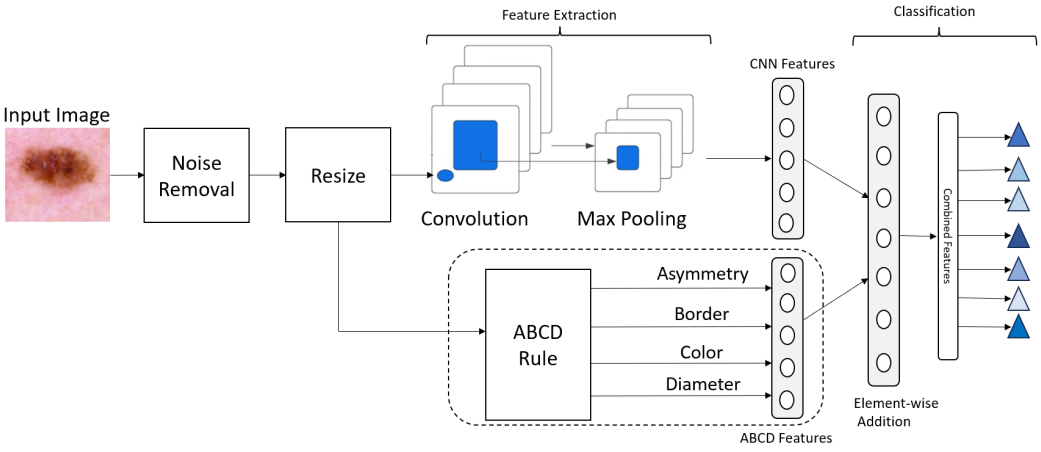

FIGURE 5. A high-level overview of CNN – ABCD rule architecture.

shows the wrong classification of the negative sample as positive by the model. Conversely, a false-negative shows the wrong classification of the positive sample as negative. The evaluation metrics that are frequently used in most classification studies are accuracy, precision, recall, and F1 score.

The accuracy is used to observe the general success of the models (Eq. (2.4)).

$$Accuracy = \frac{TP + TN}{TP + TN + FP + FN}. \tag{2.4}$$

The specificity gives the model capability to correctly predict the inputs without a disease. The formula of the specificity is given in Eq. (2.5).

$$Precision = \frac{TN}{TN + FP}. \tag{2.5}$$

Contrary to the specificity, recall is used to measure the ability of the models to predict the input samples with a disease correctly. The formula of the recall is given in Eq. (2.6).

$$Recall = \frac{TP}{TP + FN}. \tag{2.6}$$

F1-score is defined as the harmonic mean of precision and recall, as shown in Eq. (2.7).

$$F1 = 2\frac{Precision * Recall}{Precision + Recall}. \tag{2.7}$$

3. Results and Discussion

In this section, the test performances of the machine learning algorithms with the different features are given and compared. Algorithms whose performances are examined; Kernel Naïve Bayes, Cosine Similarity, Coarse KNN, Ensemble Boosted Trees, Kernel SVM, Subspace Discrimination, Cubic KNN, Ensemble Bagged Trees and Fine Tree. In the first test phase, the features obtained with the pre-trained CNN model were used. As a result of the tests using 3,005 images, the classifier with the highest accuracy was Kernel Naive Bayes with 96.3%. The Cubic KNN has the highest precision and F1 score when compared with other classifiers. In the recall value, the Coarse KNN classifier showed the best performance. The use of the Cubic KNN classifier is the optimum option in terms of overall performance since it is seen that the accuracy rate of the Cubic KNN classifier, which performs the best in Precision and F1 Score values, is 96.2% and its recall value is at a sufficient level. The results and confusion matrix obtained in all classifiers for the features obtained with the pre-trained CNN are given in Table 3 and Fig. 6, respectively.

To increase the classification accuracy, different features were given to the classifiers with different combinations and the results were compared. First, the Jaccard index related to asymmetry and color features in the ABCD rule were added to the pre-trained CNN features. According to the results obtained, the best accuracy of 96.4% was obtained in the Cosine Similarity classifier. The best results were obtained in precision and F1 score, as well as accuracy, with the Cosine Similarity classifier. In addition to the features obtained with pre-trained CNN, when the Jaccard distance and color score values are given to the input, the results obtained in all classifiers are given in Table 3. The confusion matrix of the results is given in Fig. 7.

Table 1. Results for the features obtained with the pre-trained CNN model.

	Accuracy (%)	*Precision (%)*	*Recall (%)*	*F1 Score (%)*
Kernel Naïve Bayes	**96,3**	**92,5**	**93,9**	**93,2**
Cosine Similarity	96,2	92,6	94,1	93,0
Coarse KNN	94,2	91,0	95,2	93,0
Ensemble Boosted Trees	96,2	92,8	93,0	92,9
Kernel SVM	96,2	92,6	94,4	93,5
Subspace Discriminant	96,1	92,8	94,9	93,8
Cubic KNN	96,2	92,9	94,8	93,8
Ensemble Bagged Trees	95,6	92,5	93,1	92,8
Fine Tree	93,9	91,4	91,1	91,3

TABLE 2. Results for the features obtained with the pre-trained CNN model combined with Jaccard distance and color.

	Accuracy (%)	*Precision (%)*	*Recall (%)*	*F1 Score (%)*
Kernel Naïve Bayes	96,3	92,5	93,7	93,1
Cosine Similarity	**96,4**	**93**	**93,7**	**93,4**
Coarse KNN	96,2	92,8	93,1	93,0
Ensemble Boosted Trees	96,0	92,8	94,7	93,7
Kernel SVM	96,1	92,7	94,9	93,8
Subspace Discriminant	96,1	92,5	94,7	93,6
Cubic KNN	95,4	92,5	92,8	92,6
Ensemble Bagged Trees	93,9	90,9	91,9	91,4
Fine Tree	94,2	90,8	95,4	93,0

Another test was performed to reveal the effect of other features in the ABCD rule on classification accuracy. In addition to the features obtained with pre-trained CNN, when Jaccard index, Katz Fractal Dimension related to border irregularity, diameter and color score values are given to the input, the results obtained in all classifiers are given in Table 3. According to the results obtained, there was no significant difference in the best classification accuracy compared to the results in Table 3 and the confusion matrix is given in Fig. 8. The Cosine Similarity classifier again had the highest accuracy with 96.4%. Similar results were obtained in other evaluation criteria and classifier performances.

When the results obtained in the study are evaluated in general, it has been seen that the use of features obtained with pre-trained CNN for skin lesion classification can perform classification with high accuracy. It has been shown

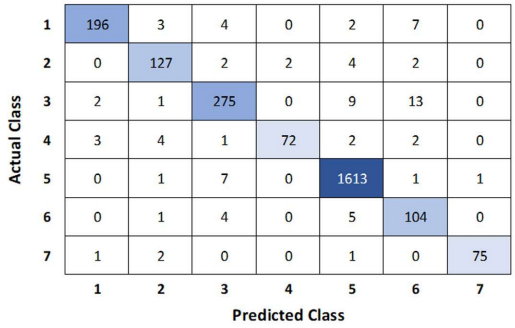

FIGURE 6. Confusion matrix for the results with features obtained via pre-trained CNN model.

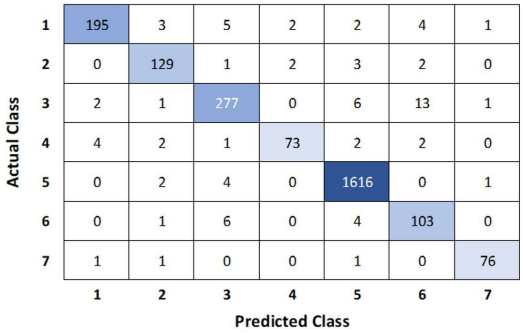

FIGURE 7. Confusion matrix for the results with features obtained via pre-trained CNN model combined with Jaccard distance and color.

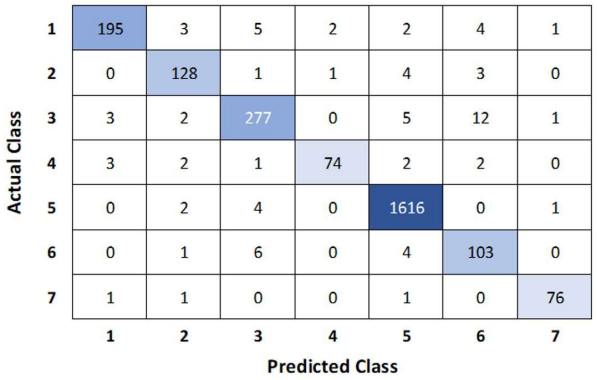

FIGURE 8. Confusion matrix for the results with features obtained via pre-trained CNN model and other eight features.

that adding the Jaccard distance and color score values in the ABCD rule to these features has a positive effect on accuracy. Besides, adding the Katz fractal dimension related to border irregularity and diameter values to these values did not make a significant difference.

4. CONCLUSIONS

With the early diagnosis of skin cancer, one of the most common diseases in the world, serious consequences can be prevented. Deep learning-based solutions are used to solve such problems. In this study, a model for the classification of seven types of skin lesions was developed by combining the features of CNN-based feature extraction and the ABCD rule, which is widely used in the clinic. The classification results obtained with different combinations of features and nine different machine learning algorithms were compared. Our future work will be focused on incorporating more models in the ensemble process with different segmentation techniques.

CONFLICTS OF INTEREST

The authors declare that there are no conflicts of interest regarding the publication of this article.

AUTHORS CONTRIBUTION STATEMENT

The authors have read and agreed to the published version of the manuscript.

TABLE 3. Results for the features obtained with the pre-trained CNN model and other eight features.

	Accuracy (%)	*Precision (%)*	*Recall (%)*	*F1 Score (%)*
Kernel Naïve Bayes	95,6	92,1	92,9	92,5
Cosine Similarity	**96,4**	**93,1**	**93,7**	**93,4**
Coarse KNN	96,3	93,4	93,2	93,3
Ensemble Boosted Trees	96,0	93,0	94,9	93,9
Kernel SVM	96,1	92,9	95,0	93,9
Subspace Discriminant	95,9	91,5	94,9	93,2
Cubic KNN	95,9	92,4	93,3	92,9
Ensemble Bagged Trees	94,1	90,7	90,3	90,5
Fine Tree	94,2	90,8	95,4	93,0

References

[1] Slaper, H., Velders, G.J., Daniel, J.S., de Gruijl, F.R., van der Leun, J.C., *Estimates of ozone depletion and skin cancer incidence to examine the Vienna Convention achievements*, Nature, **21**(1996), 256–8.

[2] Leiter, U., Eigentler, T., Garbe, C., *Epidemiology of skin cancer*, Adv Exp Med Biol., **810**(2014), 120–140.

[3] Didona, D., Paolino, G., Bottoni, U., Cantisani, C., *Non-Melanoma Skin Cancer Pathogenesis Overview*, Biomedicines, **6**(2018), 6.

[4] Barton, V., Armeson, K., Hampras, S., Ferris, L.K., Visvanathan, K. et al., *Nonmelanoma skin cancer and risk of all-cause and cancer-related mortality: a systematic review*, Arch Dermatol Res, **309**(2017), 243–251.

[5] Chung, S., *Basal cell carcinoma*, Arch Plast Surg, **39**(2012), 166–170.

[6] Ray, A., Gupta, A., Al, A., *Skin lesion classification with deep convolutional neural network: process development and validation*, JMIR Dermatol, **3**(2020), 18438.

[7] Zambrano-Román, M., Padilla-Gutiérrez, J.R., Valle, Y., Muñoz-Valle, J.F., Valdés-Alvarado, E., *Non-melanoma skin cancer: A genetic update and future perspectives*, Cancers, **14**(2022), 2371.

[8] Arnold, M., Singh, D., Laversanne, M., *Global burden of cutaneous melanoma in 2020 and projections to 2040*, JAMA Dermatol, **158**(2022), 495-–503.

[9] Balch, C.M., Gershenwald, J.E., Soong, S.J., Thompson, J.F., Atkins, M.B. et al., *Final version of 2009 AJCC melanoma staging and classification*, Journal of clinical oncology, **27**(2009), 6199.

[10] Lee, C.S., Thomas, C.M., Ng, K.E., *An overview of the changing landscape of treatment for advanced melanoma*, Pharmacotherapy, **37**(2017), 319–333.

[11] Bhatia, S., Tykodi, S.S., Thompson, J.A., *Treatment of metastatic melanoma: an overview*, Oncology, **23**(2009), 488–496.

[12] Tyrell, R., Antia, C., Stanley, S., Deutsch, G.B., *Surgical resection of metastatic melanoma in the era of immunotherapy and targeted therapy*, Melanoma Manag, **4**(2017), 61–68.

[13] Crosby, D., Lyons, N., Greenwood, E., Harrison, S., Hiom, S. et al., *A roadmap for the early detection and diagnosis of cancer*, The Lancet Oncology, **21**(2020), 1397–1399.

[14] Alendar, F., Drljević, I., Drljević, K., Alendar, T., *Early detection of melanoma skin cancer*, Bosn J Basic Med Sci, **9**(2009), 77–80.

[15] Esteva, A., Kuprel, B., Novoa, R.A., Ko, J., Swetter, S.M. et al. *Dermatologist-level classification of skin cancer with deep neural networks*, Nature, **542**(2017), 115–118.

[16] Haenssle, H.A., Fink, C., Schneiderbauer, R., Toberer, F., Buhl, T. et al., *Man against machine: diagnostic performance of a deep learning convolutional neural network for dermoscopic melanoma recognition in comparison to 58 dermatologists*, Ann Oncol, **29**(2018), 1836–1842.

[17] Tschandl, P., Rinner, C., Apalla, Z., Argenziano, G., Codella, N. et al., *Human-computer collaboration for skin cancer recognition*, Nature Medicine, **26**(2020), 1229–1234.

[18] Stanley, R.J., Stoecker, W.V., Moss, R.H., *A relative color approach to color discrimination for malignant melanoma detection in dermoscopy images*, Skin Res. Technol, **13**(2007), 62–72.

[19] Ballerini, L., Fisher, R.B., Aldridge, B., Rees, J., A Color and Texture Based Hierarchical K-NN Approach to the Classification of Non-Melanoma Skin Lesions, Color Medical Image Analysis, New York, 2013.

[20] Stoecker, W.V., Wronkiewiecz, M., Chowdhury, R., Stanley, R.J., Xu, J. et al., *Detection of granularity in dermoscopy images of malignant melanoma using color and texture features*, Comput Med Imaging Graph, **35**(2011), 144–7.

[21] Celebi, M.E., Kingravi, H.A., Uddin, B., Iyatomi H, Aslandogan Y.A. et al. *A methodological approach to the classification of dermoscopy images*, Comput Med Imaging Graph, **31**(2007), 362–373.

[22] Krizhevsky, A., Sutskever, I., Hinton, G.E., *Imagenet classification with deep convolutional neural networks*, Communications of the ACM, **60**(2017), 84–90.

[23] Shin, H.C., Roth, H.R., Gao, M., Lu, L., Xu, Z. et al., *Deep convolutional neural networks for computer-aided detection: CNN architectures dataset characteristics and transfer learning*, IEEE Trans. Med. Imag, **35**(2016), 1285–1298.

[24] Dandan, Z., Yang, L., Hongpeng, Y., Zhiqiang, W., *A novel multi-scale CNNs for false positive reduction in pulmonary nodule detection*, Expert Systems with Applications, **207**(2022), 117652.

[25] Mutasa, S., Sun, S., Ha, R., *Understanding artificial intelligence based radiology studies: CNN architecture*, Clinical Imaging, **80**(2021), 72–76.

[26] Schwendicke, F., Golla, T., Dreher, M., Krois, J., *Convolutional neural networks for dental image diagnostics: A scoping review*, Journal of Dentistry, **91**(2019), 103226.

[27] Codella, N., Cai, J., Abedini, M., Garnavi, R., Halpern, A. et al., Deep Learning, Sparse Coding, and SVM for Melanoma Recognition in Dermoscopy Images, Machine Learning in Medical Imaging, Springer, 2015.

[28] Yu, L., Chen, H., Dou, Q., Qin, J., Heng, P.A., *Automated melanoma recognition in dermoscopy images via very deep residual networks*, IEEE Transactions on Medical Imaging, **36**(2017), 994–1004.

[29] Majtner, T., Yildirim-Yayilgan, S., Hardeberg, J.Y., *Optimised deep learning features for improved melanoma detection*, Multimed Tools Appl, **78**(2019), 11883-–11903.

[30] Acosta, M.F.J., Tovar, L.Y.C., Garcia-Zapirain, M.B., Percybrooks, W.S., *Melanoma diagnosis using deep learning techniques on dermatoscopic images*, BMC Med Imaging, **21**(2021), 6.

[31] Afza, F., Sharif, M., Mittal, M., Khan, M.A., Hemanth, D.J., *A hierarchical three-step superpixels and deep learning framework for skin lesion classification*, Methods, **202**(2022), 88–102.

[32] Jin, Q., Cui, H., Sun, C., Meng, Z., Su, R., *Cascade knowledge diffusion network for skin lesion diagnosis and segmentation*, Applied Soft Computing, **99**(2021), 106881.

[33] Tschandl, P., Rosendahl, C., Kittler, H., *The HAM10000 dataset, a large collection of multi-source dermatoscopic images of common pigmented skin lesions*, Sci. Data, **5**(2018), 180161.

[34] Senan, E., Jadhav, M., *Analysis of dermoscopy images by using ABCD rule for early detection of skin cancer*, Global Transitions Proceedings,**2**(2021), 1–7.

[35] Cheng, H.D., Shan, J., Ju, W., Guo, Y., Zhang, L., *Automated breast cancer detection and classification using ultrasound images: A survey*, Pattern Recognition, **43**(2010), 299—317.

[36] Chollet, F., *Xception: Deep learning with depthwise separable convolutions*, Proceedings of the IEEE Conference on Computer Vision and Pattern Recognition, (2017), 1251–1258.

[37] Liu, Y., Zhang, L., Hao, Z., Yang, Z., Wang, S. et al., *An Xception model based on residual attention mechanism for the classification of benign and malignant gastric ulcers*, Sci Rep, **12**(2022), 15365.

[38] Moataz, L., Salama, G., Elazeem, M., *Skin cancer diseases classification using deep convolutional neural network with transfer learning model*, Journal of Physics: Conference Series, (2021), 2128.

[39] Lu, X., Zadeh, Y.A., *Deep Learning-Based Classification for Melanoma Detection Using XceptionNet*, Journal of Healthcare Engineering, (2022), 1–10.

[40] Coye, T., Novel Method for Determining Symmetry of Skin Lesions using the Jaccard Index, MATLAB Central File Exchange, 2015, (https://www.mathworks.com/matlabcentral/fileexchange/50903-novel-method-for-determining-symmetry-of-skin-lesions-using-the-jaccard-index), Retrieved January 3, 2023.

[41] Katz, M.J., *Fractals and the analysis of waveforms*, Computers in Biology and Medicine, **18**(1988), 145-–156.

[42] Chatterjee, S., Dey, D., Munshi, S., *Optimal selection of features using wavelet fractal descriptors and automatic correlation bias reduction for classifying skin lesions*, Biomedical Signal Processing and Control, **40**(2018), 252–262.

[43] Chatterjee, S., Dey, D., Munshi, S., Gorai, S., *Dermatological expert system implementing the ABCD rule of dermoscopy for skin disease identification*, Expert Systems with Applications, **167**(2021), 114204.

[44] Coye, T., Tyler Coye (2023). Function for Counting Colors in a Skin Lesion, MATLAB Central File Exchange, 2015, (https://www.mathworks.com/matlabcentral/fileexchange/50872-function-for-counting-colors-in-a-skin-lesion), Retrieved January 4, 2023.